Published online: March 3, 2017

Article

TRANSPARENT PROCESS OPEN ACCESS

THE EMBO JOURNAL

Uncoupling of neurogenesis and differentiation during retinal development

Peter Engerer[1], Sachihiro C Suzuki[2,‡], Takeshi Yoshimatsu[2,§], Prisca Chapouton[3], Nancy Obeng[1], Benjamin Odermatt[4], Philip R Williams[1,¶,†,*], Thomas Misgeld[1,5,6,7,†,**] & Leanne Godinho[1,†,***]

Abstract

Conventionally, neuronal development is regarded to follow a stereotypic sequence of neurogenesis, migration, and differentiation. We demonstrate that this notion is not a general principle of neuronal development by documenting the timing of mitosis in relation to multiple differentiation events for bipolar cells (BCs) in the zebrafish retina using *in vivo* imaging. We found that BC progenitors undergo terminal neurogenic divisions while in markedly disparate stages of neuronal differentiation. Remarkably, the differentiation state of individual BC progenitors at mitosis is not arbitrary but matches the differentiation state of post-mitotic BCs in their surround. By experimentally shifting the relative timing of progenitor division and differentiation, we provide evidence that neurogenesis and differentiation can occur independently of each other. We propose that the uncoupling of neurogenesis and differentiation could provide neurogenic programs with flexibility, while allowing for synchronous neuronal development within a continuously expanding cell pool.

Keywords bipolar cells; development; differentiation; neurogenesis; retina
Subject Categories Development & Differentiation; Neuroscience
DOI 10.15252/embj.201694230 | Received 1 March 2016 | Revised 17 January 2017 | Accepted 24 January 2017

Introduction

The nervous system is indisputably the most complex structure assembled during vertebrate ontogenesis. Consequently, the developmental processes underlying nervous system assembly must be precisely orchestrated. Neuronal development in the central and peripheral nervous systems (CNS, PNS) is widely accepted to require three major steps: (i) neurogenesis, the birth of neurons by progenitor cell mitosis, (ii) migration, the relocation of post-mitotic neurons from their birthplace in proliferative zones to specific locations, and (iii) neuronal differentiation, the acquisition of molecular and morphological features that permit the integration of newly generated neurons into synaptic circuits. To date, the prevailing view is that these ontogenetic events are discrete steps along a stereotypic sequence, beginning with neurogenesis, followed by migration and concluding with neuronal differentiation. There is however, particularly in the PNS, evidence that some hallmarks of neuronal differentiation might already occur in progenitors (Rothman *et al*, 1980; Rohrer & Thoenen, 1987; DiCicco-Bloom *et al*, 1990; Godinho *et al*, 2007; Attardo *et al*, 2008). These observations call into question the invariant developmental sequence of neurogenesis, migration, and differentiation, and raise the unresolved question: How stereotypic is the developmental program of a defined progenitor population *in vivo*?

Here, we examined the developmental fate of a molecularly defined CNS progenitor population (expressing *visual homeobox gene 1*, *vsx1*) that gives rise to the vast majority of a specific interneuron cell type (bipolar cells, BCs) in the zebrafish retina by terminal symmetric divisions (He *et al*, 2012; Weber *et al*, 2014). The swift development as well as the genetic and optical accessibility of zebrafish permitted us to follow the entire developmental program of *vsx1*$^{+}$ progenitors, with single cell precision, *in vivo*. We used molecular, morphological, and cell biological markers of neuronal differentiation, in conjunction with chronic *in vivo* time-lapse imaging, to determine the timing of mitosis in relation to a battery of developmental events. We discovered that for BCs, neurogenesis and multiple hallmarks of neuronal differentiation (such as

1 Institute of Neuronal Cell Biology, Technische Universität München, Munich, Germany
2 Department of Biological Structure, University of Washington, Seattle, Washington, USA
3 Sensory Biology and Organogenesis, German Research Center for Environmental Health, Helmholtz Zentrum München, Neuherberg, Germany
4 Anatomisches Institut, Rheinische Friedrich-Wilhelms-Universität Bonn, Bonn, Germany
5 Center of Integrated Protein Science (CIPSM), Munich, Germany
6 German Center for Neurodegenerative Diseases (DZNE), Munich, Germany
7 Munich Cluster of Systems Neurology (SyNergy), Munich, Germany
*Corresponding author. Tel: +1 617 919 2271; E-mail: philip.williams@childrens.harvard.edu
**Corresponding author. Tel: +49 89 41403330; E-mail: thomas.misgeld@tum.de
***Corresponding author. Tel: +49 89 41403331; E-mail: leanne.godinho@tum.de
† These authors contributed equally to this work
‡ Present address: Technology Licensing Section, Okinawa Institute of Science and Technology, Graduate University, Okinawa, Japan
§ Present address: Sussex Neuroscience, School of Life Sciences, University of Sussex, Brighton, UK
¶ Present address: Department of Neurology, F.M. Kirby Neurobiology Center, Children's Hospital of Boston, Harvard Medical School, Boston, MA, USA

somal positioning, neuronal marker expression, or neurite elaboration) are timed independently of each other. In other words, rather than dividing at a stereotypic point in their developmental trajectory, *vsx1*$^+$ progenitors of BCs undergo terminal mitosis at markedly disparate stages of differentiation, suggesting that differentiation is not time-locked to mitosis. However, the state of differentiation of a *vsx1*$^+$ progenitor at mitosis is not arbitrary, but matches that of the post-mitotic *vsx1*$^+$ BCs in its vicinity.

Results

Bipolar cell progenitor mitoses occur over an extended time-period and relocate to non-apical sites

In common with many parts of the developing vertebrate CNS, the retina begins as a pseudostratified neuroepithelium with spindle-shaped progenitors that span its apico-basal extent and undergo interkinetic nuclear migration, an oscillatory nuclear movement linked to specific cell cycle phases (Sauer, 1935; Baye & Link, 2008). At distinct but overlapping times, cells destined for different fates exit the cell cycle. Because mitotic divisions generally occur at the apical surface, newborn cells need to migrate varying distances to occupy their definitive locations within one of the emerging cellular laminae. Thus, while ganglion cells migrate furthest to occupy positions in the basal most part of the neuroepithelium, BCs have a shorter distance to relocate, and photoreceptors remain *in situ* at the apical surface. BCs, which are ultimately localized to the inner nuclear layer (INL) and confine their dendritic and axonal processes to the outer and inner plexiform layers (OPL, IPL), respectively, are generated over a protracted period, between 2 and 3 days post-fertilization (dpf) in the zebrafish (He *et al*, 2012). Thus, early-born cohorts of BCs are generated when the retinal neuroepithelium is not yet laminated, while later-born cohorts are generated when the three cellular laminae are emerging.

To investigate the relationship between BC neurogenesis and differentiation, we examined the expression of *vsx1*, a transcription factor important for BC development (Passini *et al*, 1997; Chow *et al*, 2001; Vitorino *et al*, 2009; Shi *et al*, 2011), using a *vsx1*:GFP transgenic line (Kimura *et al*, 2008). In the zebrafish retina, *vsx1* is expressed at low levels in the majority of committed, terminally dividing BC progenitors, up-regulated during differentiation, and maintained at high levels in mature BCs (Vitorino *et al*, 2009). This developmental expression profile is faithfully reproduced in the bacterial artificial chromosome (BAC) *vsx1*:GFP transgenic line (Vitorino *et al*, 2009), so that we could follow nascent BCs from birth to maturity. Further, we took advantage of the zebrafish retina's gradient of development (Hu & Easter, 1999), to concurrently visualize immature (unlaminated) and more mature (laminated) parts of the retina and thus compare multiple states of BC differentiation in a single field of view.

At 2 dpf, we found low levels of GFP expression in the unlaminated part of the retina in which *vsx1*:GFP$^+$ (henceforth referred to as *vsx1*$^+$) cells span the entire apico-basal axis. These *vsx1*$^+$ cells represent both BC progenitors and post-mitotic, undifferentiated BCs (Morgan *et al*, 2006; Randlett *et al*, 2013). By contrast, *vsx1*$^+$ cells in the more mature, laminated part of the retina showed high levels of GFP expression and confined their processes to the IPL and OPL, suggestive of post-mitotic, differentiated BCs (Fig 1A). To our surprise, immunostaining of *vsx1*:GFP retinas for phosphorylated histone H3 (pH3), a late G_2/M-phase marker (Hendzel *et al*, 1997), revealed *vsx1*$^+$ pH3$^+$ cells not only in the unlaminated retina but also in the INL of the laminated retina. This suggests that not only post-mitotic BCs but also *vsx1*$^+$ progenitors reside within the INL (Fig 1A–D). Notably, while *vsx1*$^+$ progenitors in the unlaminated retina undergo mitosis at the apical surface, like "classical" progenitors in many parts of the CNS (Fig 1B), *vsx1*$^+$ progenitors in the laminated retina undergo mitosis in the INL (Fig 1C), akin to previously described non-apical progenitors (Godinho *et al*, 2007; Weber *et al*, 2014). Given the precocious expression of some neuronal characteristics in such non-apical progenitors, we asked how similar *vsx1*$^+$ progenitors were to the post-mitotic *vsx1*$^+$ BCs in their immediate surround.

Marker expression in progenitors matches the surrounding post-mitotic bipolar cells

GFP levels during mitotic division in *vsx1*$^+$ pH3$^+$ progenitors showed a striking (3.8-fold) increase between the unlaminated and laminated regions of the developing retina (Fig 1E), which

Figure 1. *Vsx1*$^+$ progenitors undergo mitosis in different proliferative zones and match the expression of molecular markers of post-mitotic BCs in their vicinity.

A Confocal images of a coronal cryostat section from a 2 dpf *vsx1*:GFP retina with immature, neuroepithelial ("unlaminated", orange) and mature, laminated regions ("laminated", cyan). Left panel, *vsx1*:GFP; right panel, *vsx1*:GFP shown in conjunction with pH3 antibody staining to label cells in late G_2/M-phase. Scale bar: 10 μm.

B, C High magnification images of (B) an apically dividing *vsx1*$^+$ progenitor (orange arrowhead) in an unlaminated region where cells span the retina and express GFP weakly and (C) a non-apically dividing *vsx1*$^+$ progenitor (cyan arrowhead) in a laminated region where cells confine their processes to the OPL and IPL (dashed lines) and express high levels of GFP. Cellular membranes are labeled with BODIPY methyl ester. Scale bar: 10 μm.

D Quantification of *vsx1*$^+$ progenitor mitoses at apical (lightly shaded) and non-apical (darkly shaded) locations in the unlaminated ("un", orange) and laminated ("lam", cyan) retina. Data are presented as mean ± SEM, 1,391 mitotic divisions, 80 sections from at least 14 fish.

E Quantification of *vsx1*:GFP fluorescence intensity in dividing *vsx1*$^+$ progenitors in the unlaminated ("un", orange) and laminated ("lam", cyan) retina. Data are presented as mean ± SEM, 86 progenitors, 43 sections from at least 13 eyes, Mann–Whitney *U*-test, ***$P \leq 0.0001$.

F Correlation of *vsx1*:GFP fluorescence intensity in progenitors and their surrounding cells in the unlaminated (orange circles) and laminated (cyan circles) regions of the retina. Eighty-six progenitors from 43 sections from at least 13 eyes, $r^2 = 0.78$. Inset: Analysis for all pH3$^+$ cells ($n = 13$) from a single section.

G Confocal images of a cryostat section from a 2 dpf *vsx1*:GFP retina immunostained with antibodies against pH3 and Crx. *Vsx1*$^+$ progenitors (GFP$^+$ pH3$^+$) are Crx negative (orange arrowheads) in the unlaminated retina (left panels, orange bars above panels) and are Crx positive (cyan arrowhead) in the laminated region (right panels, cyan bars above panels). Scale bar: 10 μm.

H Correlation of Crx antibody staining intensity between mitotic BC progenitors and the *vsx1*$^+$ cells in their vicinity. Thirty-eight progenitors, 10 sections from at least five eyes, $r^2 = 0.87$; orange circles, apical mitoses; cyan circles, non-apical mitoses.

Published online: March 3, 2017

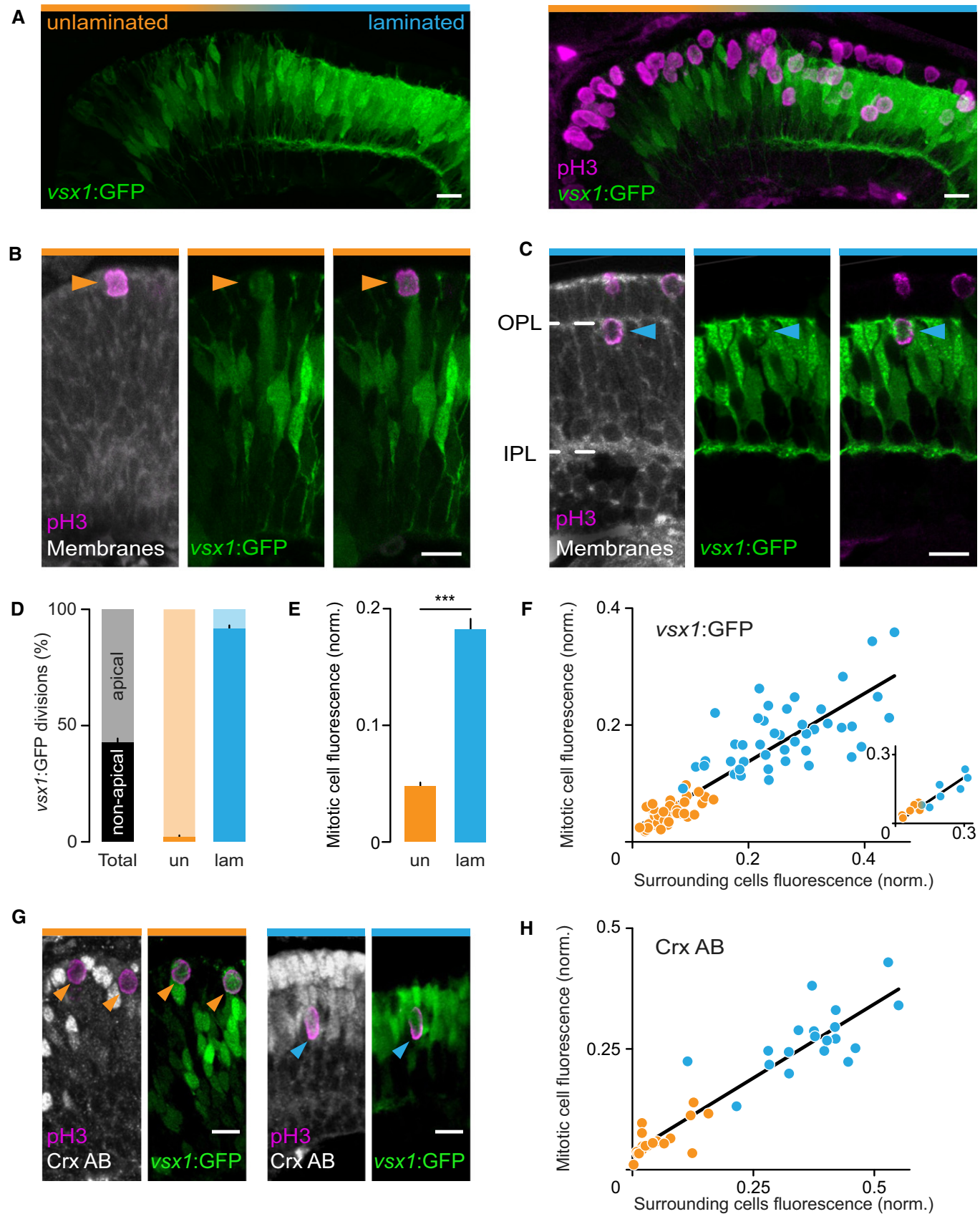

Figure 1.

correlated well with the GFP levels in surrounding *vsx1*$^+$ pH3$^-$ cells (Fig 1F; the surrounding *vsx1*$^+$ cells in laminated regions are expected to be ~90% post-mitotic BCs on average; for an estimate of this number see Appendix Supplementary Materials and Methods). Furthermore, comparison of *vsx1*:GFP levels in pH3$^+$ progenitors and pH3$^-$ surrounding cells across the entire developmental gradient in single retinas revealed a linear increase along the gradient (Fig 1F, inset). Hence, with regard to *vsx1* expression, progenitors in the laminated retina are more similar to their BC neighbors than to their early dividing peers and form a continuum with regard to *vsx1* promoter activity in lock-step with surrounding BC differentiation. Direct time-lapse observation of *vsx1*:GFP levels confirmed a parallel increase of fluorescence levels in BC progenitors and surrounding post-mitotic BCs *in vivo* (Fig EV1). Moreover, based on the decay of GFP in a *vsx2*:GFP BAC line (Vitorino *et al*, 2009), *vsx2* down-regulation was similarly linked to the progression of differentiation along the retinal gradient independent of mitotic status.

To further establish this similarity in molecular differentiation of *vsx1*$^+$ progenitors and their post-mitotic neighbors, we examined two additional molecular markers of BC differentiation: cone-rod homeobox (Crx) and Ribeye a. Crx is a transcription factor expressed in mature photoreceptors and BCs (Liu *et al*, 2001; Shen & Raymond, 2004). In the unlaminated retina, antibody staining for

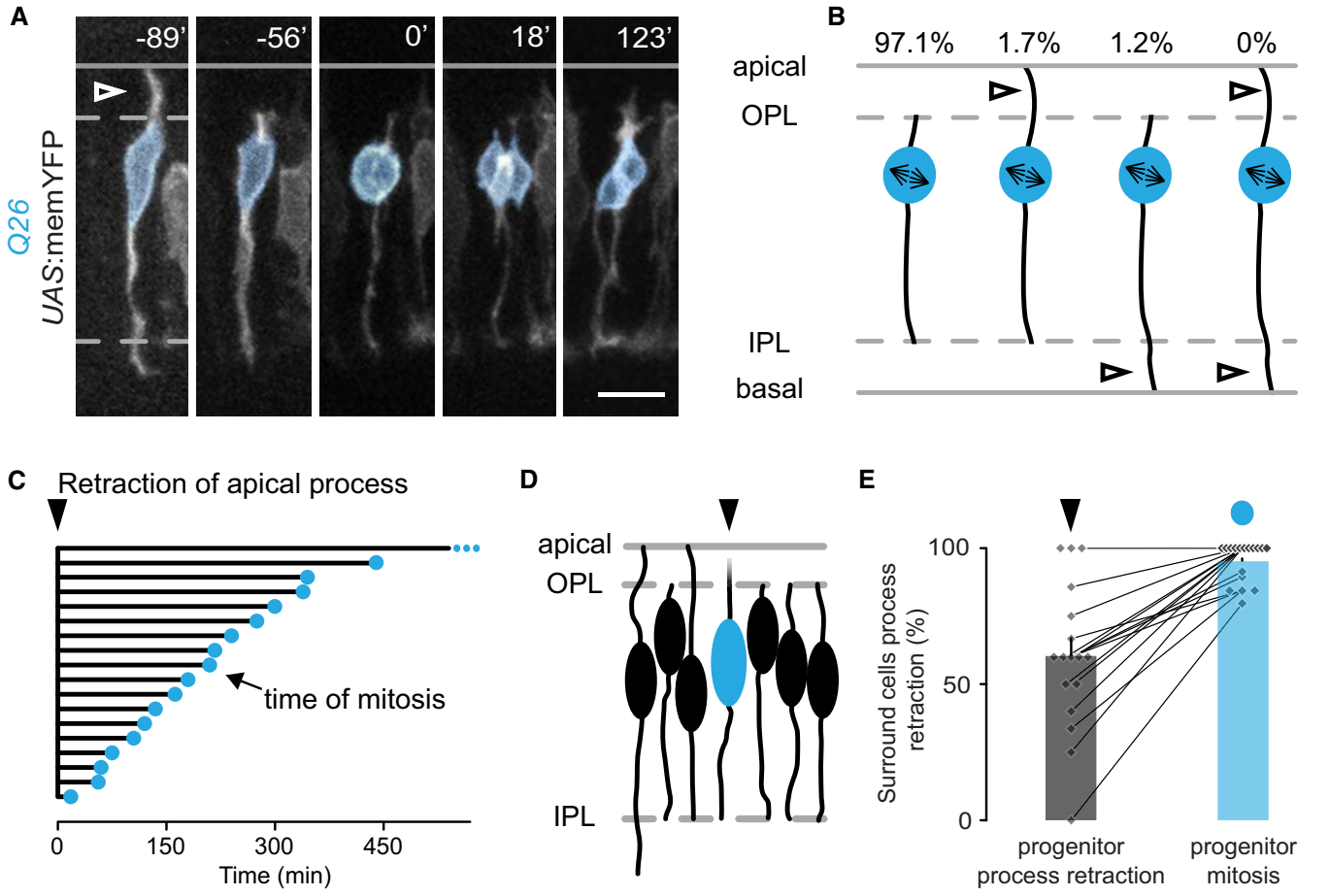

Figure 2. Morphological rearrangement of *vsx1*$^+$ progenitors matches surrounding BCs.

A Confocal *in vivo* time-lapse recording of a retina from the *Q26* transgenic line (crossed to a *UAS*:memYFP reporter) showing a non-apically dividing *vsx1*$^+$ progenitor (pseudo-colored cyan) with processes restricted to the IPL and OPL (dashed lines) during mitosis (0'). The last time point at which an apical process (open arrowhead) is detected is 89 min prior to mitosis. Scale bar: 10 μm.

B Quantification of the distinct morphologies adopted by non-apically dividing *vsx1*$^+$ progenitors at M-phase entry (122 progenitors, 17 fish). Open arrowheads indicate cytoplasmic processes extending beyond the synaptic layers (OPL and IPL, dashed lines).

C Quantification of the time interval between retraction of the apical process (triangle) and mitosis (cyan circle) of non-apically dividing *vsx1*$^+$ progenitors shows a broad range from 18 min to more than 540 min. As only mitosis, but not process retraction was observed for the progenitor depicted with small cyan dots, the movie length of 540 min is an underestimate. 18 progenitors from 11 fish.

D Schematic of apical process retraction (triangle) in a non-apical *vsx1*$^+$ progenitor (cyan soma) and the presence or absence of apical processes in the surrounding, post-mitotic BCs.

E Quantification of the percentage of surrounding post-mitotic BCs without an apical process at the time when pre-mitotic *vsx1*$^+$ progenitors undergo apical process retraction (triangle, 60.3 ± 6.6%) and at the time when these progenitors undergo mitosis (cyan circle, 95.1 ± 1.7%). Data are presented as mean ± SEM, 17 progenitors, 10 fish.

Crx (combined with pH3) revealed little or no expression in *vsx1*$^+$ progenitors or the *vsx1*$^+$ cells in their vicinity, whereas in laminated regions, high levels of Crx expression were found in virtually all *vsx1*$^+$ progenitors and surrounding post-mitotic *vsx1*$^+$ BCs (Fig 1G). The levels of Crx antibody staining in mitotic *vsx1*$^+$ progenitors along the differentiation gradient strongly correlated with that of the *vsx1*$^+$ cells in their immediate surround (Fig 1H). Moreover, time-lapse imaging of a *crx*:mCFP transgenic line (Suzuki *et al*, 2013), in which Crx$^+$ cells are faithfully labeled (Fig EV2A), regularly revealed non-apical *crx*:mCFP$^+$ mitotic divisions in the laminated retina (Fig EV2B and C). Finally, we analyzed the expression of Ribeye a, a structural protein of ribbon synapses in photoreceptors and BCs (Wan *et al*, 2005). As expected, using fluorescence *in situ* hybridization, we found *ribeye a* mRNA only in the laminated retina, where post-mitotic cells predominate (Fig EV2D and E). Notably, we also observed *ribeye a* mRNA-containing cells that were pH3$^+$ (Fig EV2F). The fact that these cells were located in the INL suggests they are BC progenitors. Using a transgenic line designed to report *ribeye a* expression in BCs (*ctbp2*:mEGFP; Odermatt *et al*, 2012), we observed *ctbp2*:mEGFP$^+$ cells dividing at non-apical locations, giving rise to BCs (Fig EV2G). Hence, even with regard to a marker linked to synaptic structures unique to BCs in the inner retina, we find that BC progenitors co-differentiate with post-mitotic BCs in the surround. We next asked whether this similarity extended beyond molecular markers to cellular morphology and dynamics.

Progenitor morphology and cell biology correspond to the surrounding post-mitotic bipolar cells

To examine individual cells of the *vsx1*$^+$ BC lineage, we generated a transgenic Gal4-driver line (referred to as *Q26*) that was selected to label a sparse subset of *vsx1*$^+$ cells. As Gal4 expression in *Q26* is restricted to *vsx1*$^+$ BCs and their progenitors in laminated parts of the retinal gradient (Appendix Fig S1), we almost exclusively observed non-apically dividing *Q26*$^+$ progenitors, which we followed by time-lapse imaging as they terminally divided to produce BCs (Fig 2A). We examined the cleavage plane in dividing *Q26*$^+$ progenitors (n = 65) and found divisions along the circumferential, apico-basal, and centro-peripheral axes with no preference for a particular orientation, in line with other reports of non-apically dividing progenitors (Kimura *et al*, 2008; Weber *et al*, 2014). During mitosis, the vast majority of *Q26*$^+$ progenitors had limited their processes to the plexiform layers (Fig 2A at 0′, Fig 2B), as is characteristic for BCs in the mouse and zebrafish retina (Morgan *et al*, 2006; Randlett *et al*, 2013) but not for apically dividing progenitors (Das *et al*, 2003; Miyata *et al*, 2004; Noctor *et al*, 2004). Prior to mitotic division however, the processes of non-apically dividing progenitors extended beyond the OPL or IPL (see Fig 2A at −89′) and over time remodeled to become restricted to the synaptic layers. We asked whether this morphological remodeling occurred in a fixed time-window relative to mitotic division and focused our analyses, for technical reasons (see Appendix Supplementary Materials and Methods) on the retraction of processes from the apical surface. We found that apical process retraction occurred over an extended period of time (18 min to > 9 h) prior to mitotic division (Fig 2C). In contrast, for apically dividing BC progenitors in the unlaminated retina, apical process retraction to the OPL was a post-mitotic event (as observed in *vsx1*:GFP), but again occurred over an extended time span following mitotic division (a few min to > 8 h). Thus, a single differentiation step, the remodeling of the apical process, occurs both pre- and post-mitotically, and over a time span of more than 17 h relative to mitosis. Notably however, our time-lapse recordings in the *Q26* line suggested that apical process remodeling is locally coordinated. When we identified progenitors that had just undergone apical process retraction to the OPL and asked whether post-mitotic BCs in the immediate vicinity had also done the same (Fig 2D), we found that, on the population level, apical process remodeling occurred concurrently (Fig 2E). Moreover, once pruned, the apical and basal processes of pre-mitotic progenitors could form lateral arbors. While these arbors regressed during mitosis, at earlier time points we could not distinguish them from the dendritic and axonal arbors of surrounding post-mitotic BCs (brackets in Fig 3A and E; Fig 4D at −645′), suggesting that the morphological processes of BC differentiation proceed independent of progenitor mitosis. In accordance with observations from other systems and species (Miyata *et al*, 2001; Das *et al*, 2003; Saito *et al*, 2003; Kosodo *et al*, 2008) the basally directed process of dividing *Q26*$^+$ progenitors exhibited either splitting or asymmetric inheritance by one daughter cell followed by new outgrowth by the other daughter (Appendix Fig S2). Remarkably, when new process outgrowth was observed, it exhibited directed targeting of the IPL without overshooting beyond it.

Next, we asked whether *vsx1*$^+$ progenitors undergo interkinetic nuclear migration. We used an mRNA construct encoding a fusion

Figure 3. *Vsx1*$^+$ progenitors in the unlaminated and laminated region exhibit distinct cell biological behaviors.

A Concurrent visualization of nucleokinesis in a *vsx1*$^+$ progenitor in the laminated retina (*Q26*; *UAS*:memYFP, upper panels) and the cell cycle stage (mOrange2-PCNA mRNA, lower panels) by *in vivo* time-lapse confocal imaging. Progenitor soma is pseudo-colored cyan in YFP channel and outlined in cyan in mOrange channel. Scale bar: 10 μm.

B Nuclear movement of *vsx1*$^+$ progenitors in the unlaminated region (*vsx1*:GFP) of the retina prior to mitosis at the apical surface (orange circle). Seven cells, five fish. Black line represents the average position of all *vsx1*$^+$ progenitors prior to mitosis in unlaminated regions.

C Nuclear trajectories of *vsx1*$^+$ progenitors in the laminated region that undergo mitosis at the INL/OPL interface (cyan circle, left panel) and post-mitotic BCs in their vicinity (right panel). In the time interval during which trajectories were tracked, all 12 *vsx1*$^+$ progenitors move to the INL/OPL interface prior to mitosis; 8 of 12 post-mitotic surrounding BCs do so (five fish). Black lines represent the average position of all *vsx1*$^+$ progenitors prior to mitosis in laminated regions (left panel) or of the post-mitotic BCs (right panel).

D Centrosomes (centrin4-YFP mRNA, grayscale) of a *vsx1*$^+$ progenitor (magenta mask, *Q19*) and post-mitotic BCs in the laminated region concurrently translocate to the OPL and remain clustered there. The centrosome of the highlighted *vsx1*$^+$ progenitor is pseudo-colored green. Scale bar: 10 μm.

E Continuation of the time-lapse from (D) (centrosomes not depicted). The *vsx1*$^+$ progenitor (magenta mask) shows transient lateral arborizations in the synaptic layers as wide as its soma (see brackets at −210′, −165′). A further example can be seen in (A) (see brackets at −67′).

protein between mOrange2 and proliferating cell nuclear antigen (PCNA; Fig 3A and Appendix Fig S3) that allows determination of progenitor cell cycle phase by distinct nuclear localization patterns (Leonhardt *et al*, 2000; Leung *et al*, 2011). Similar to classical progenitors, *vsx1*$^{+}$ progenitors in the unlaminated region exhibited rapid apically directed interkinetic nuclear migration during G_2

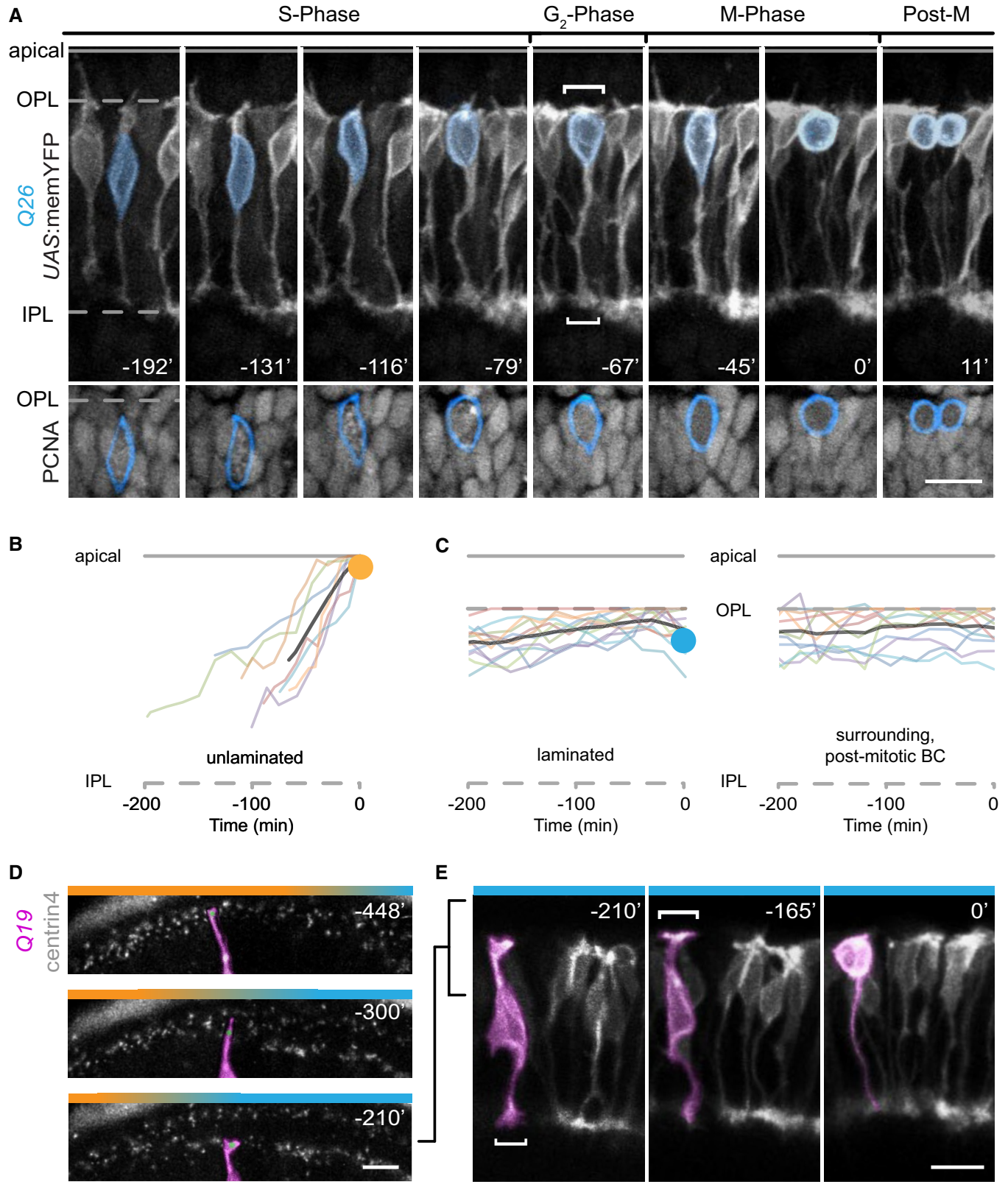

Figure 3.

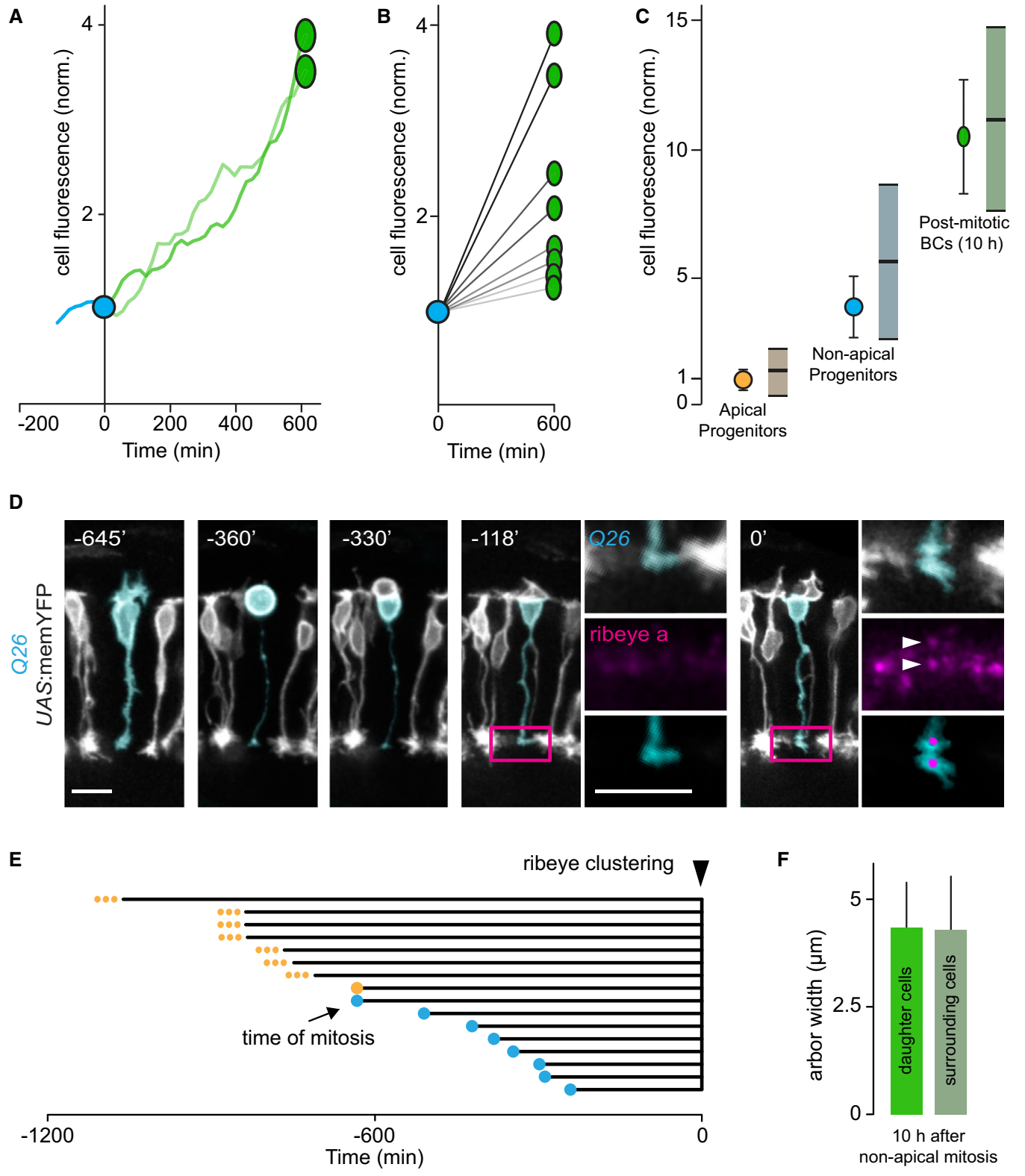

Figure 4.

before mitosis at the apical surface (Fig 3B and Appendix Fig S3). This movement was absent in non-apically dividing *vsx1*$^{+}$ progenitors, making their nuclear movements largely indistinguishable from the post-mitotic BCs in their immediate vicinity (Fig 3A and C). However, the non-apically dividing *vsx1*$^{+}$ progenitors always translocated their nuclei to the INL/OPL interface prior to mitosis. This movement can be explained by the location of the centrosome. By expressing fluorescently tagged centrin4, we found that BC

Figure 4. The differentiation status of late-born bipolar cells and earlier-born bipolar cells in their vicinity are similar.

A Fluorescence intensity of a non-apically dividing *vsx1*$^+$ progenitor before it undergoes mitotic division (cyan trace), at the time of mitotic division (cyan circle) and of the two BC daughter cells (green ovals) over the course of 10 h (green traces).

B Quantification of the fluorescence intensity of four pairs of BC daughters (green ovals) derived from non-apically dividing *vsx1*$^+$ progenitors (cyan circle) 10 h after division. The fluorescence intensity of each of the BC pairs was normalized to the mitotic cell from which they were derived. BC pairs depicted are derived from two fish. The different overall rates of GFP fluorescence increase can be explained by where along the differentiation gradient cells originate.

C Comparison of the *vsx1* expression levels of apical progenitors, non-apical progenitors, and post-mitotic BCs derived from non-apically dividing progenitors 10 h following division. The fluorescence expression levels of cells surrounding each of the three cell categories are also quantified. Apically dividing *vsx1*$^+$ progenitors (orange circle) and surrounding cells (dull orange bar, mean, and standard deviation, SD). Non-apically dividing *vsx1*$^+$ progenitors (cyan circle) and surrounding cells (dull cyan bar, mean, and SD). In total, 43 apically dividing progenitors and 524 cells in their surround, and 43 non-apically dividing progenitors and 521 cells in their surround from at least 13 eyes were used for this analysis. Post-mitotic BCs (green oval) and earlier-born surrounding cells (dull green bar, mean, and standard deviation). Eleven post-mitotic BCs derived from seven mitotic divisions and 105 cells in their surround from three fish were used for this analysis.

D Confocal *in vivo* time-lapse recording of the emergence of ribeye a puncta (pseudo-colored magenta, *ctbp2*:mCherry-ctbp2) in a BC derived from a non-apically dividing *vsx1*$^+$ progenitor (pseudo-colored cyan, *Q26*; *UAS*:memYFP), 7 h following cell cycle exit. Insets of the magenta-boxed region (at −118′ and 0′) of the axon terminal of the BC reveal the emergence of discernible ribeye a puncta at the 0′ time point (white arrowheads). Scale bars: 10 μm.

E Quantification of the time interval between mitosis and clustering of ribeye puncta (triangle) in the axon terminals of the ensuing BC daughters. Eight BCs derived from seven non-apically dividing progenitors (cyan circles) and eight BCs derived from apically dividing *vsx1*$^+$ progenitors (orange circles) from three fish were used for this analysis. In seven of the eight BCs derived from apical progenitors (depicted as small orange dots), we observed clustering but not the mitotic division, thus the time interval in these cases is an underestimate.

F Quantification of the axon terminal arbor width of BCs derived from non-apical *vsx1*$^+$ progenitors and the cells in their surround. At 10 h post-division, mean arbor width for BCs was 4.34 ± 1.05 μm, SD; the mean arbor width for cells in their surround was 4.29 ± 1.24 μm, SD. In total, nine BCs derived from seven non-apical divisions and 56 surround cells from six fish were used for analysis.

centrosomes actively relocated from the apical surface to the INL/OPL interface (Fig 3D and E), resulting in a dendritic, rather than a somatic location at maturity (Fig EV3). Like apical process retraction, centrosome relocation occurred at the same time for progenitors and surrounding, post-mitotic BCs (Figs 3D and EV3). Thus, nucleokinesis and centrosome relocation represent further differentiation steps for which *vsx1*$^+$ progenitors are time-locked to their post-mitotic neighbors.

The post-mitotic differentiation status of late-born bipolar cells is similar to the early-born bipolar cell population in their vicinity

We assessed the rate of differentiation of the BC progeny resulting from non-apically dividing *vsx1*$^+$ progenitors in the laminated region of the retina. First, we monitored *vsx1*-driven GFP expression levels in post-mitotic BCs over the course of 10 h after their exit from the cell cycle and found a steady increase in fluorescence intensity (Fig 4A). Ten hours post-division, GFP expression levels in BC sibling pairs were remarkably similar to each other (Fig 4A and B) and remained similar to the cells in their surround, which largely comprised of earlier-born post-mitotic BCs (Fig 4C).

Next, we used an established transgenic line, *ctbp2*:mCherry-ctbp2 (Pelassa *et al*, 2014), to examine the emergence of ribbon synapses in BC axon terminals. We assessed the time interval between exit from the cell cycle and the appearance of ribeye a clusters (marker of ribbon synapses) as an indication of presynaptic differentiation in *vsx1*$^+$ BCs (Fig 4D). For late-born BCs derived from non-apically dividing *vsx1*$^+$ progenitors, the average time interval was 6.5 h. By contrast, for early-born BCs this interval was longer than 13 h on average (Fig 4E). Thus, late-born BCs acquire features of presynaptic differentiation with greater speed than their earlier-born counter-parts. Finally, we measured the lateral extent of the terminal axonal arbors of BCs derived from non-apical *vsx1*$^+$ progenitors 10 h after they exited the cell cycle, and found this to be remarkably similar to that of the earlier-born post-mitotic BCs in their vicinity (Fig 4F). Taken together, late-born BCs continue to differentiate in lock-step with earlier-born BCs in their vicinity, including the elaboration of markers of axonal and synaptic differentiation, thus contributing to synchrony in local neuronal development.

Experimentally delaying cell division does not delay *vsx1*$^+$ progenitor differentiation

Our experiments have established that along the developmental gradient, BC progenitors blend into the differentiation landscape that surrounds them with regard to their morphological, cell biological, and molecular characteristics. Moreover, the "head-start" gained by pre-mitotic differentiation in late-dividing progenitors continues in their BC progeny, so that the lag in differentiation between late-born and early-born BCs is remarkably low. Two potential scenarios could explain these observations: (i) Multiple, "fixed" *vsx1*$^+$ progenitors exist, each of which undergoes mitosis at a stereotypic time point in the cell's differentiation trajectory. (ii) Alternatively, neurogenesis and differentiation could be uncoupled from each other, so that mitotic divisions could occur at various points in any given *vsx1*$^+$ cell's differentiation program. To distinguish between these two possibilities, we delayed BC progenitor divisions using hydroxyurea and aphidicolin (HUA). HUA treatment rapidly reduced the number of cells entering the G_2/M-phase (Appendix Fig S4), but a small number of progenitors continued to divide, albeit with a prominent delay. We could now ask whether during delayed progenitor mitosis, differentiation stalled (as implied by the existence of "fixed" progenitors) or whether it continued and remained in synchrony with surrounding post-mitotic BC differentiation (as predicted by the "uncoupling" scenario; Fig 5A). We tracked 10 *vsx1*$^+$ progenitors in HUA-treated embryos from late S-phase until mitosis. Knowing that progenitors, in control experiments, divided on average 142 ± 3.9 min after the onset of late S-phase, we could determine when a HUA-treated cell should have divided ("expected" mitosis) and measured the delay with which the division actually occurred ("observed" mitosis, delay range approximately 3.5–9 h; Figs 5B and EV4). Because we could predict with a high degree of accuracy (86.4%), whether progenitors, in control conditions, would undergo mitosis at the apical surface or in the INL well before the divisions occurred (see

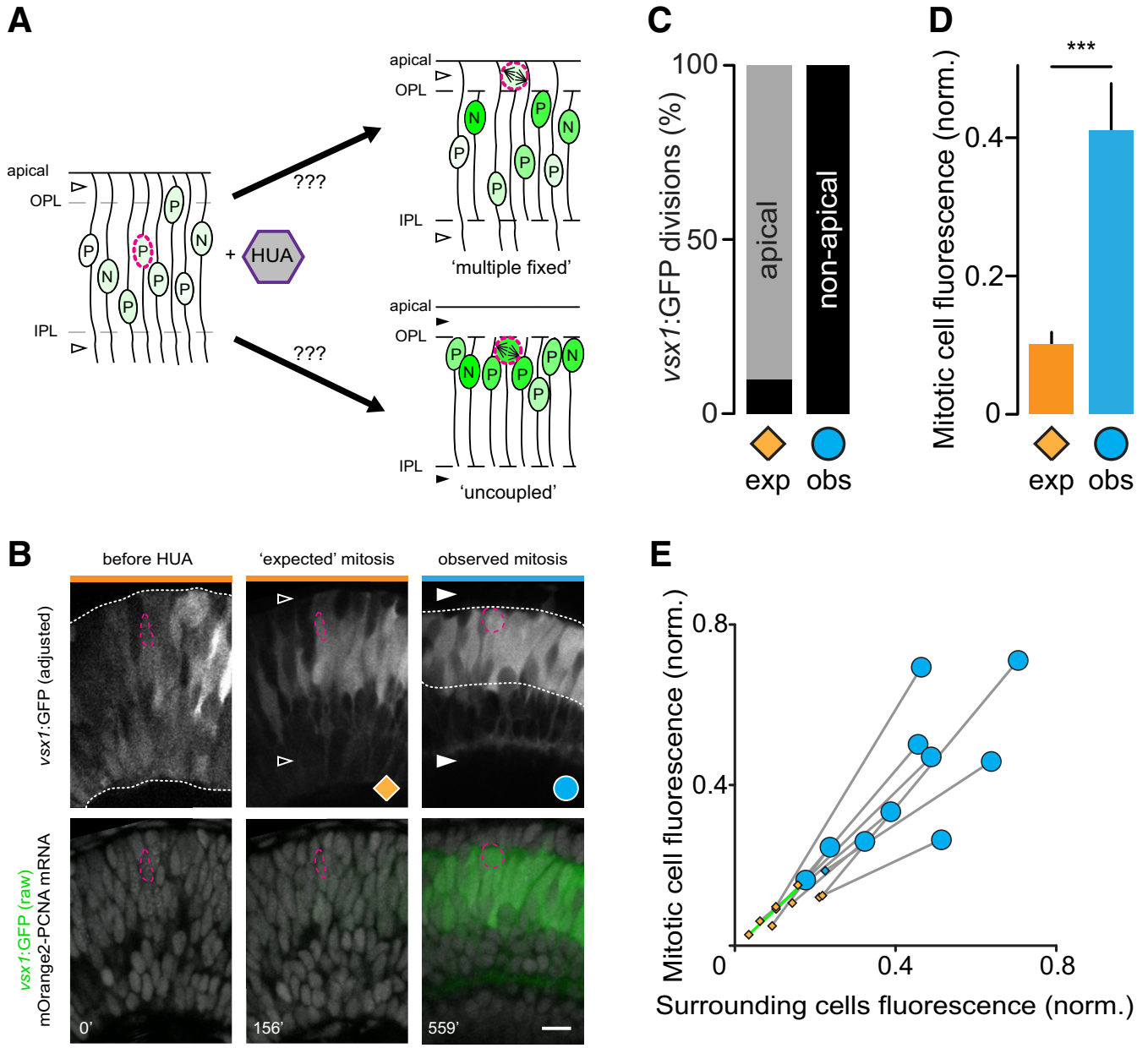

Figure 5. Neurogenesis and differentiation of *vsx1*$^+$ progenitors are independent of each other.

A Schematic representation of expected outcomes if the immature retina (progenitors, P; neurons, N) is treated with HUA to delay the cell cycle. Upper panel: If there are multiple "fixed" progenitors, a block of cell division should stall progenitors at the differentiation state in which they normally would have undergone mitosis. The result would be a "salt-and-pepper" pattern of undifferentiated (light green) and differentiating progenitors (dark green). Lower panel: If cell cycle and differentiation are independent, all progenitors should homogenously differentiate. Open arrowheads indicate cytoplasmic processes not confined to the OPL and IPL, filled arrowheads indicate cytoplasmic processes confined to the synaptic layers.

B Confocal images of a 2 dpf retina from a *vsx1*:GFP embryo injected with a p53 morpholino and mOrange2-PCNA mRNA. A *vsx1*$^+$ progenitor (dashed magenta outline) is shown before HUA treatment (left panel), at the time when it would have been "expected" to undergo mitosis (middle panel, orange diamond) and when it actually underwent mitosis (right panel, cyan circle). The retina and the *vsx1*$^+$ progenitor continue to mature after the "expected" mitosis (retraction of cytoplasmic processes, mitosis at non-apical location, and up-regulation of GFP). Open arrowheads indicate cytoplasmic processes not confined to the OPL and IPL, filled arrowheads indicate cytoplasmic processes confined to the synaptic layers. Dotted lines indicate extent of *vsx1*$^+$ cell somata across retinal thickness. Scale bar: 10 μm.

C Progenitors that were expected to divide at the apical surface (exp), divided non-apically (obs). 10 progenitors, four fish.

D Quantification of *vsx1*:GFP fluorescence intensity of progenitors at the time when they were expected to undergo mitosis (exp, orange) and when they underwent mitotic division (obs, cyan). Data are presented as mean ± SEM, 10 progenitors, four fish. Mann–Whitney *U*-test, ***P = 0.0002.

E The fluorescence intensity of HUA-treated *vsx1*:GFP progenitors at the time when they were expected to undergo mitosis (diamonds), and when they were observed to undergo mitosis (circles), plotted against the intensity of the surrounding cells (10 progenitors, four fish). One cell (cyan diamond) was expected to divide non-apically. Green line indicates the fluorescence change of the lowest expressing progenitor for clarity.

Appendix Supplementary Materials and Methods), we could ask whether the HUA-induced delay of mitosis would shift divisions from apical to non-apical locations (as an "uncoupling" scenario would imply). Nine of the 10 HUA-treated cells fulfilled criteria that identified them to be destined to divide apically. However, all 10 cells instead underwent mitosis in the INL after process remodeling, suggesting that they had been shifted from an apical to a non-apical phenotype simply by delaying mitosis (Fig 5C). Furthermore, *vsx1*:GFP expression levels in the 10 delayed progenitors increased from the point of expected mitosis to observed mitosis (Fig 5D). Notably, even hours after the delayed mitosis occurred, progenitors still matched the fluorescence levels of cells in their immediate surround (Fig 5E), suggesting uncoupling of cell division and differentiation. Together, these findings support the "uncoupling" scenario laid out above and hence argue for an independence of neurogenesis and differentiation programs during BC development.

Discussion

Our study is the first, to our knowledge, to address the relative timing of neurogenesis, migration, and differentiation for a molecularly defined CNS population *in vivo* and to elucidate the effects of such timing on progenitor characteristics. In contrast to the widely held view, we found that developing neurons did not adopt a stereotypic sequence of neurogenesis followed by migration and subsequent differentiation. Rather, to our surprise, the developmental trajectories that progenitors adopted were variable and accommodated remarkable flexibility. This resulted in *vsx1*$^{+}$ BC progenitors with a wide variety of molecular, morphological, and cell biological characteristics. Importantly, rather than representing many distinct populations, the differentiation status of these progenitors formed a continuum in lock-step with the differentiation of surrounding post-mitotic BCs along the developmental gradient of the retina. Accordingly, cells dividing in the laminated parts of the retina were more BC-like than their early dividing counter-parts. Indeed, without the aid of time-lapse imaging or cell cycle markers it would have been impossible to distinguish between pre-mitotic progenitors and post-mitotic cells. Our results support the conclusion that a stereotypical and fixed sequence of ontogenetic events is not essential during neuronal development. Thus, at least for terminally dividing progenitors, which generate a substantial part of the CNS neuronal population (Nakashima *et al*, 2015), mitosis does not have to occur before neuronal differentiation is initiated (or at any specific step thereafter), but rather can be flexibly intercalated between other developmental steps.

Our findings could explain two previous intriguing observations: First, that neuronal progenitors in different parts of the nervous system show precocious signs of differentiation prior to cell cycle exit (Rothman *et al*, 1980; Rohrer & Thoenen, 1987; DiCicco-Bloom *et al*, 1990; Miyata *et al*, 2004; Godinho *et al*, 2007; Attardo *et al*, 2008; Prasov & Glaser, 2012); and second, that blocking mitosis does not halt neuronal differentiation in many parts of the *Xenopus* CNS including the retina, spinal cord, and brain stem (Harris & Hartenstein, 1991). Our results now offer a unifying explanation for these previous observations, suggesting that they might simply result from a fundamental uncoupling of cell cycle and neuronal differentiation during normal development. Indeed, the increasingly recognized prevalence of precocious progenitors in many parts of the nervous system of a range of species [e.g., basal progenitors in the neocortex (Haubensak *et al*, 2004; Miyata *et al*, 2004; Noctor *et al*, 2004); neural crest-derived PNS progenitors (Rothman *et al*, 1980; Rohrer & Thoenen, 1987; DiCicco-Bloom *et al*, 1990); retinal progenitors (Godinho *et al*, 2007; Prasov & Glaser, 2012)], implies that such uncoupling may be a general principle of neural development.

What would be the advantages of uncoupling neurogenesis and neuronal differentiation? By comparison with the orderly sequence of developmental events in the classical model, we suggest that the uncoupled model provides two advantages, namely speed and synchrony (Fig EV5). In the classical model, because differentiation can only be initiated following mitosis, the time required for the majority of cells in a defined population to differentiate is dictated by the delay in their birth dates. By contrast, in the uncoupled model, differentiation steps can already occur at the progenitor stage, permitting differentiation across the population to be faster. Furthermore, despite the extended time span over which mitotic divisions can occur, cells in a given population differentiate in relative synchrony. The uncoupling of mitosis and differentiation could thus be particularly pertinent for the assembly of essential neural circuits where swift maturation is paramount for survival (Nikolaou & Meyer, 2015).

Materials and Methods

Animals

All experiments were performed according to regulations as approved by the local regulatory bodies. Zebrafish were maintained, mated, and raised as described in Mullins *et al* (1994). Embryos were kept in 0.3× Danieau's solution at 28.5°C and staged as previously described (Kimmel *et al*, 1995). Fish were either in an AB wild-type or *roy orbison* (Ren *et al*, 2002) background. The transgenic lines used are listed in Appendix Table S1. We generated Tg (*vsx1*:Gal4)q26 (*Q26*) and Tg(14x*UAS*:memTagRFP-T) by Tol2 mediated insertion (Kawakami, 2004). For details of constructs used to make transgenic fish and for transient injections see Appendix Supplementary Materials and Methods.

mRNA synthesis and injection

Plasmids were linearized (PCNA: NotI, centrin4: ApaI). Capped mRNA was produced using the Ambion mMESSAGE mMACHINE kit (Applied Biosystems) according to the manufacturer's instructions. mRNA was injected at 100 ng/μl into one- or two-cell stage embryos.

Immunohistochemistry and *in situ* hybridization

Immunostaining to detect pH3, Crx, and GFP was performed using adaptations of previously published protocols either on cryosections (Williams *et al*, 2010) or on whole-mount embryos (Hunter *et al*, 2011). *In situ* hybridization to visualize *ribeye a* mRNA was performed on whole-mount embryos using a digoxigenin-labeled riboprobe and Fast Red TR/naphthol AS-MX (Sigma) to detect alkaline phosphatase activity. For a detailed description see Appendix Supplementary Materials and Methods.

In vivo imaging

Embryos were prepared for imaging as described previously (Godinho, 2011; Engerer *et al*, 2016). Between 10 and 18 h post-fertilization (hpf), embryos were transferred to 0.3× Danieau's solution containing 0.003% 1-phenyl-2-thiourea (PTU, Sigma) to inhibit melanin formation. At 2.25 days post-fertilization (dpf), manually dechorionated embryos were anesthetized using 0.02% tricaine (PharmaQ) in medium containing PTU and embedded laying on their side in low-melting agarose (0.7–0.8%, Sigma).

Fish were imaged starting at 2 dpf on an Olympus FV1000 confocal/2-photon and an Olympus FVMPE-RS 2-photon microscope using water-immersion objectives (Olympus 20×/NA 0.95, Olympus 25×/NA 1.05, Zeiss 40×/NA 1.0, Nikon 25×/NA 1.1, and Nikon 40×/NA 0.8) or a silicon-immersion objective (Olympus 30×/NA 1.05). Embryos were maintained at 28.5°C during all *in vivo* recordings. At each time point *z*-stacks were acquired of the peripheral retina, encompassing its entire circumference.

Image processing

Images were viewed and processed using open-source ImageJ/Fiji software (http://fiji.sc). The StackReg function was used for drift compensation in xy. Image panels were assembled in Photoshop CS5 (Adobe) and combined into figures using Illustrator CS5 (Adobe). The "Gaussian blur" function was used to filter noise for clarity. Gamma was not adjusted.

Hydroxyurea-aphidicolin treatment

Hydroxyurea (Sigma) and aphidicolin (BioViotica) were used at a final concentration of 20 mM and 150 μM, respectively, in 0.3× Danieau's containing 1.0–1.7% DMSO. Embryos were injected with a p53 morpholino (0.5–1 mM, Gene Tools) at the one- or two-cell stage to ameliorate HUA-induced apoptosis (Girdler *et al*, 2013). At 2 dpf embryos were mounted in agarose as described for *in vivo* imaging above, but leaving the tail fin un-embedded for better drug access. Retinas were imaged for one time point prior to HUA administration. The 0.3× Danieau's medium was replaced with HUA-containing medium, and time-lapse recording was immediately resumed. Recordings were generally limited to < 16 h after HUA addition as high levels of cell death were observed thereafter.

Data analysis

For details, see Appendix Supplementary Materials and Methods.

Statistics

Mean values and standard error of the mean (SEM) were calculated using Microsoft Excel. We used the Mann–Whitney *U*-test to compare datasets with GraphPad Prism 5. Data are presented as mean ± SEM unless indicated otherwise. *P*-values < 0.05 are denoted with "*", $P < 0.01$ with "**", and $P < 0.001$ with "***".

Expanded View for this article is available online.

Acknowledgements
We thank Kristina Wullimann for expert fish husbandry and Yvonne Hufnagel, Alexandra Graupner, and Monika Schetterer for expert technical and administrative support. We are especially grateful to Rachel Wong (U. Washington, Seattle), who generously supported this project in multiple ways, thanks to her, and Magdalena Götz and Tim Czopka for critical reading of an earlier version of this manuscript. We are grateful to M. Nonet (Washington University in St. Louis) for the pCold Heart Tol2 vector, M. Meyer (King's College London) for the 5xUAS:TagRFP-T vector, T. Nicolson (Oregon Health & Science University and Vollum Institute) for the *ribeye a* cDNA template, R. Köster (Technische Universität Braunschweig) for pSK5xUAS:Centrin2-YFP, and P. Raymond (University of Michigan) for the anti-Crx antibody. The mOrange2-PCNA-19-SV40NLS-4 plasmid was a gift from Michael Davidson (Addgene plasmid # 57971). We thank S. Higashijima (National Institutes of Natural Sciences, Okazaki Institute for Integrative Bioscience) for the Tg(vsx1:GFP)nns5 and Tg(vsx2:GFP)nns1 BAC transgenic lines which were generated with the support of the National Bioresource Project of Japan. We also thank R. Wong for providing the following transgenic lines: Tg(*pax6-DF4*:gap43-CFP)q01, Tg(*vsx1*:MCerulean)q19, Tg(*14xUAS*:MYFP), and Tg(*crx*:MA-CFP)q20, and L. Lagnado (University of Sussex, UK) for Tg(*−1.8ctbp2a*:mCherry-ctbp2a)lmb7. The Tg(*−1.8ctbp2*:gap43-EGFP)lmb1 line was made in the laboratory of L. Lagnado at MRC-LMB, Cambridge. This project was made possible by funding to L.G. and T.M. from the Deutsche Forschungsgemeinschaft (DFG) through Collaborative Research Center 870 "Assembly and Function of Neuronal Circuits", project A11. T.M. is further supported by the Center for Integrated Protein Science Munich (CIPSM, EXC 114), the European Research Council under the European Union's Seventh Framework Program (FP/2007-2013; ERC Grant Agreement no. 616791), the Munich Center for Systems Neurology (SyNergy; EXC 1010), the DFG Priority Program 1710 (Mi694/4-1), the DFG research grants Mi694/7-1, 8-1, and the German-Israeli Foundation (I-1200-237.1/2012). T.M. is also associated with the German Center for Neurodegenerative Diseases (DZNE Munich). P.R.W. was supported by the Human Frontier Science Program and the Wings for Life Foundation. N.O. was supported by the Amgen Scholar program. S.C.S. and T.Y. were supported by a grant awarded to R. Wong (NIH EY14358). P.E. was supported by the DFG Research Training Group 1373 and the Graduate School of the Technische Universität München (TUM-GS).

Author contributions
PE, PRW, TM, and LG conceived of the project and designed experiments. TM and LG supervised the project. PE performed all *in vivo* imaging experiments, with some help from NO. PE and PC performed *in situ* hybridization. PE, SCS, TY, NO, and BO generated new constructs and transgenic lines for this research. PE, PRW, TM, and LG wrote the paper with input from all authors.

Conflict of interest
The authors declare that they have no conflict of interest.

References

Attardo A, Calegari F, Haubensak W, Wilsch-Brauninger M, Huttner WB (2008) Live imaging at the onset of cortical neurogenesis reveals differential appearance of the neuronal phenotype in apical versus basal progenitor progeny. *PLoS One* 3: e2388

Baye LM, Link BA (2008) Nuclear migration during retinal development. *Brain Res* 1192: 29–36

Chow RL, Snow B, Novak J, Looser J, Freund C, Vidgen D, Ploder L, McInnes RR (2001) Vsx1, a rapidly evolving paired-like homeobox gene expressed in cone bipolar cells. *Mech Dev* 109: 315 – 322

Das T, Payer B, Cayouette M, Harris WA (2003) *In vivo* time-lapse imaging of cell divisions during neurogenesis in the developing zebrafish retina. *Neuron* 37: 597 – 609

DiCicco-Bloom E, Townes-Anderson E, Black IB (1990) Neuroblast mitosis in dissociated culture: regulation and relationship to differentiation. *J Cell Biol* 110: 2073 – 2086

Engerer P, Plucinska G, Thong R, Trovo L, Paquet D, Godinho L (2016) Imaging subcellular structures in the living zebrafish embryo. *J Vis Exp* 110: e53456

Girdler GC, Araya C, Ren X, Clarke JD (2013) Developmental time rather than local environment regulates the schedule of epithelial polarization in the zebrafish neural rod. *Neural Dev* 8: 5

Godinho L, Williams PR, Claassen Y, Provost E, Leach SD, Kamermans M, Wong RO (2007) Nonapical symmetric divisions underlie horizontal cell layer formation in the developing retina *in vivo*. *Neuron* 56: 597 – 603

Godinho L (2011) Live imaging of zebrafish development. *Cold Spring Harb Protoc* 2011: 770 – 777

Harris WA, Hartenstein V (1991) Neuronal determination without cell division in *Xenopus* embryos. *Neuron* 6: 499 – 515

Haubensak W, Attardo A, Denk W, Huttner WB (2004) Neurons arise in the basal neuroepithelium of the early mammalian telencephalon: a major site of neurogenesis. *Proc Natl Acad Sci USA* 101: 3196 – 3201

He J, Zhang G, Almeida AD, Cayouette M, Simons BD, Harris WA (2012) How variable clones build an invariant retina. *Neuron* 75: 786 – 798

Hendzel MJ, Wei Y, Mancini MA, Van Hooser A, Ranalli T, Brinkley BR, Bazett-Jones DP, Allis CD (1997) Mitosis-specific phosphorylation of histone H3 initiates primarily within pericentromeric heterochromatin during G2 and spreads in an ordered fashion coincident with mitotic chromosome condensation. *Chromosoma* 106: 348 – 360

Hu M, Easter SS (1999) Retinal neurogenesis: the formation of the initial central patch of postmitotic cells. *Dev Biol* 207: 309 – 321

Hunter PR, Nikolaou N, Odermatt B, Williams PR, Drescher U, Meyer MP (2011) Localization of Cadm2a and Cadm3 proteins during development of the zebrafish nervous system. *J Comp Neurol* 519: 2252 – 2270

Kawakami K (2004) Transgenesis and gene trap methods in zebrafish by using the Tol2 transposable element. *Methods Cell Biol* 77: 201 – 222

Kimmel CB, Ballard WW, Kimmel SR, Ullmann B, Schilling TF (1995) Stages of embryonic development of the zebrafish. *Dev Dyn* 203: 253 – 310

Kimura Y, Satou C, Higashijima S (2008) V2a and V2b neurons are generated by the final divisions of pair-producing progenitors in the zebrafish spinal cord. *Development* 135: 3001 – 3005

Kosodo Y, Toida K, Dubreuil V, Alexandre P, Schenk J, Kiyokage E, Attardo A, Mora-Bermudez F, Arii T, Clarke JD, Huttner WB (2008) Cytokinesis of neuroepithelial cells can divide their basal process before anaphase. *EMBO J* 27: 3151 – 3163

Leonhardt H, Rahn HP, Weinzierl P, Sporbert A, Cremer T, Zink D, Cardoso MC (2000) Dynamics of DNA replication factories in living cells. *J Cell Biol* 149: 271 – 280

Leung L, Klopper AV, Grill SW, Harris WA, Norden C (2011) Apical migration of nuclei during G2 is a prerequisite for all nuclear motion in zebrafish neuroepithelia. *Development* 138: 5003 – 5013

Liu Y, Shen Y, Rest JS, Raymond PA, Zack DJ (2001) Isolation and characterization of a zebrafish homologue of the cone rod homeobox gene. *Invest Ophthalmol Vis Sci* 42: 481 – 487

Miyata T, Kawaguchi A, Okano H, Ogawa M (2001) Asymmetric inheritance of radial glial fibers by cortical neurons. *Neuron* 31: 727 – 741

Miyata T, Kawaguchi A, Saito K, Kawano M, Muto T, Ogawa M (2004) Asymmetric production of surface-dividing and non-surface-dividing cortical progenitor cells. *Development* 131: 3133 – 3145

Morgan JL, Dhingra A, Vardi N, Wong RO (2006) Axons and dendrites originate from neuroepithelial-like processes of retinal bipolar cells. *Nat Neurosci* 9: 85 – 92

Mullins MC, Hammerschmidt M, Haffter P, Nusslein-Volhard C (1994) Large-scale mutagenesis in the zebrafish: in search of genes controlling development in a vertebrate. *Curr Biol* 4: 189 – 202

Nakashima K, Umeshima H, Kengaku M (2015) Cerebellar granule cells are predominantly generated by terminal symmetric divisions of granule cell precursors. *Dev Dyn* 244: 748 – 758

Nikolaou N, Meyer MP (2015) Lamination speeds the functional development of visual circuits. *Neuron* 88: 999 – 1013

Noctor SC, Martinez-Cerdeno V, Ivic L, Kriegstein AR (2004) Cortical neurons arise in symmetric and asymmetric division zones and migrate through specific phases. *Nat Neurosci* 7: 136 – 144

Odermatt B, Nikolaev A, Lagnado L (2012) Encoding of luminance and contrast by linear and nonlinear synapses in the retina. *Neuron* 73: 758 – 773

Passini MA, Levine EM, Canger AK, Raymond PA, Schechter N (1997) Vsx-1 and Vsx-2: differential expression of two paired-like homeobox genes during zebrafish and goldfish retinogenesis. *J Comp Neurol* 388: 495 – 505

Pelassa I, Zhao C, Pasche M, Odermatt B, Lagnado L (2014) Synaptic vesicles are "primed" for fast clathrin-mediated endocytosis at the ribbon synapse. *Front Mol Neurosci* 7: 91

Prasov L, Glaser T (2012) Dynamic expression of ganglion cell markers in retinal progenitors during the terminal cell cycle. *Mol Cell Neurosci* 50: 160 – 168

Randlett O, MacDonald RB, Yoshimatsu T, Almeida AD, Suzuki SC, Wong RO, Harris WA (2013) Cellular requirements for building a retinal neuropil. *Cell Rep* 3: 282 – 290

Ren JQ, McCarthy WR, Zhang H, Adolph AR, Li L (2002) Behavioral visual responses of wild-type and hypopigmented zebrafish. *Vision Res* 42: 293 – 299

Rohrer H, Thoenen H (1987) Relationship between differentiation and terminal mitosis: chick sensory and ciliary neurons differentiate after terminal mitosis of precursor cells, whereas sympathetic neurons continue to divide after differentiation. *J Neurosci* 7: 3739 – 3748

Rothman TP, Specht LA, Gershon MD, Joh TH, Teitelman G, Pickel VM, Reis DJ (1980) Catecholamine biosynthetic enzymes are expressed in replicating cells of the peripheral but not the central nervous system. *Proc Natl Acad Sci USA* 77: 6221 – 6225

Saito K, Kawaguchi A, Kashiwagi S, Yasugi S, Ogawa M, Miyata T (2003) Morphological asymmetry in dividing retinal progenitor cells. *Dev Growth Differ* 45: 219 – 229

Sauer FC (1935) Mitosis in the neural tube. *J Comp Neurol* 62: 377 – 405

Shen YC, Raymond PA (2004) Zebrafish cone-rod (crx) homeobox gene promotes retinogenesis. *Dev Biol* 269: 237 – 251

Shi Z, Trenholm S, Zhu M, Buddingh S, Star EN, Awatramani GB, Chow RL (2011) Vsx1 regulates terminal differentiation of type 7 ON bipolar cells. *J Neurosci* 31: 13118 – 13127

Suzuki SC, Bleckert A, Williams PR, Takechi M, Kawamura S, Wong RO (2013) Cone photoreceptor types in zebrafish are generated by symmetric terminal divisions of dedicated precursors. *Proc Natl Acad Sci USA* 110: 15109 – 15114

Vitorino M, Jusuf PR, Maurus D, Kimura Y, Higashijima S, Harris WA (2009) Vsx2 in the zebrafish retina: restricted lineages through derepression. *Neural Dev* 4: 14

Wan L, Almers W, Chen W (2005) Two ribeye genes in teleosts: the role of Ribeye in ribbon formation and bipolar cell development. *J Neurosci* 25: 941 – 949

Weber IP, Ramos AP, Strzyz PJ, Leung LC, Young S, Norden C (2014) Mitotic position and morphology of committed precursor cells in the zebrafish retina adapt to architectural changes upon tissue maturation. *Cell Rep* 7: 386 – 397

Williams PR, Suzuki SC, Yoshimatsu T, Lawrence OT, Waldron SJ, Parsons MJ, Nonet ML, Wong RO (2010) *In vivo* development of outer retinal synapses in the absence of glial contact. *J Neurosci* 30: 11951 – 11961